Fine-structure anomalies in EPR spectra of Gd^{3+} centres formed in $TlCdF_3$ single crystals

2006 J. Phys.: Condens. Matter 18 7427

(http://iopscience.iop.org/0953-8984/18/31/034)

INSTITUTE OF PHYSICS PUBLISHING JOURNAL OF PHYSICS: CONDENSED MATTER

J. Phys.: Condens. Matter **18** (2006) 7427–7436 doi:10.1088/0953-8984/18/31/034

Fine-structure anomalies in EPR spectra of Gd^{3+} centres formed in $TlCdF_3$ single crystals

M Arakawa[1], F Hirayama[1], H Ebisu[2] and H Takeuchi[3]

[1] Department of Materials Science and Engineering, Nagoya Institute of Technology, Nagoya 466-8555, Japan
[2] Department of Electrical and Electronics Engineering, Nagoya Institute of Technology, Nagoya 466-8555, Japan
[3] Department of Advanced Science and Technology, Toyota Technological Institute, Nagoya 468-8511, Japan

Received 9 May 2006, in final form 5 July 2006
Published 21 July 2006
Online at stacks.iop.org/JPhysCM/18/7427

Abstract

Electron paramagnetic resonance (EPR) measurements have been made on as-grown single crystals of perovskite-type $TlCdF_3$ at room temperature in the cubic phase. Signals from two kinds of tetragonal Gd^{3+} centre are observed. One centre observed in the Gd-only-doped crystal is ascribed to a Gd^{3+} ion at a Cd^{2+} site being associated with a vacancy at the nearest Cd^{2+} site. The other centre observed in the Gd, Li co-doped crystal is ascribed to a Gd^{3+} ion at a Cd^{2+} site being associated with a Li^{+} ion at the nearest Cd^{2+} site. The fine-structure terms are discussed by separating them into the uniaxial and cubic terms. Anomalous values of the axial and cubic parameters are obtained for $TlCdF_3$ in contrast with the parameters for other host crystals $ACdF_3$ (A = K, Rb, Cs).

1. Introduction

When a trivalent magnetic ion substitutes for a host divalent cation, the excess positive charge on the magnetic ion is compensated by some defect in ionic crystals. In some cases, several kinds of magnetic centre are formed in the crystals where the magnetic ions are associated with local charge compensator in their immediate neighbourhood. Electron paramagnetic resonance (EPR) is a sensitive technique for studying such local environments around the magnetic ions with spin $S \geqslant 1$ through the fine structure of EPR spectrum. For the purpose of clarifying the low-symmetry structure around magnetic ions, the authors' group has carried out EPR investigations and found several empirical rules existing between the fine-structure parameters and the local environment of the magnetic ion by using the spin-Hamiltonian separation method. In this method we separate the fine-structure terms in the spin Hamiltonian into several tensor operator terms having uniaxial or cubic symmetries and compare the parameters for the separated terms with corresponding values for related magnetic centres.

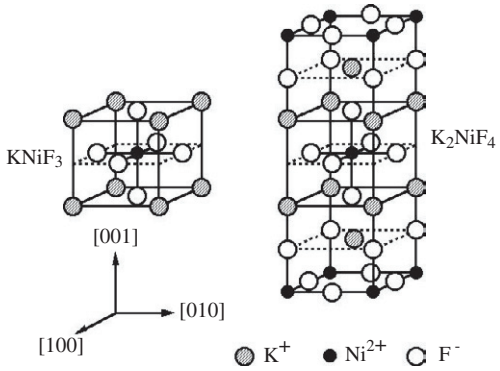

Figure 1. Unit cells of cubic perovskite ($KNiF_3$-type) and layered perovskite (K_2NiF_4-type) crystals.

Since $KNiF_3$-like cubic perovskite fluorides have advantages in their simple structure around divalent cations, many EPR studies on fine-structure terms for the magnetic ions doped in cubic perovskite fluorides have been reported [1–10]. The K_2NiF_4-like layered perovskite crystals are useful host crystals for the study of fine-structure terms by the spin-Hamiltonian separation analysis in conjunction with cubic perovskite crystals. Unit cells of a cubic and a layered perovskite-type crystal are shown in figure 1.

In some layered perovskite crystals A_2BF_4 (A = K, Rb, Cs; B = Zn, Cd) doped with M^{3+} ions (M = Cr, Fe, Gd), orthorhombic spectra of substitutional M^{3+} ions at B^{2+} sites associated with a B^{2+} vacancy (M^{3+}–V_B centre) or a Li^+ ion (M^{3+}–Li^+ centre) at the nearest B^{2+} site have been observed together with the tetragonal spectra of the substitutional M^{3+} ion at a B^{2+} site without a nearby charge compensator [11–16]. The relationship between the second-rank fine-structure parameters b_2^0, b_2^2 and the local environment around the M^{3+} ion was investigated by separating the fine-structure terms into two uniaxial terms along the c axis with the parameter $b_{2a(1)}$ and along the M^{3+}–V_B (or M^{3+}–Li^+) pair direction with the parameter $b_{2a(2)}$. The structure of the M^{3+} centre was discussed by comparing each separated axial parameter $b_{2a(1)}$ or $b_{2a(2)}$ respectively with the axial parameter b_2^0 for the M^{3+} centre without a nearby charge compensator in the same layered perovskite crystal and with the axial parameter b_2^0 for the M^{3+}–V_B centre (or M^{3+}–Li^+ centre) of the corresponding cubic ABF_3 crystal.

In the recent EPR studies for the Cr^{3+} centres [14] and for the Fe^{3+} centres [15] in thallium compounds Tl_2MgF_4 and Tl_2ZnF_4, spectra of the tetragonal M^{3+} centres showed unexpectedly large fine-structure splittings. By the spin-Hamiltonian separation analysis, the tetragonal centres were identified to be the M^{3+} centres without a nearby charge compensator having anomalously large axial parameters b_2^0, which are about double the magnitude of those in Rb_2ZnF_4 [12, 16]. The other anomaly was found in the separated axial parameter $b_{2a(2)}$ for the Cr^{3+}–V_{Zn} centre in Tl_2ZnF_4, which has about double the magnitude of those in K_2ZnF_4 [11] and Rb_2ZnF_4 [12].

It is suggested from the above results that Tl^+ ions may cause a local distortion of surrounding ions rather different from those in the crystals with other monovalent cations (K^+, Rb^+, Cs^+). So, direct observation of the anomaly caused by Tl^+ ions may be expected from EPR spectra for tetragonal M^{3+}–V_B centre and M^{3+}–Li^+ centre formed in cubic perovskite-type thallium compounds $TlBF_3$. However, $TlZnF_3$ cannot be used for this purpose as the crystal is in hexagonal $BaTiO_3$-type structure. On the other hand, $TlCdF_3$ undergoes a O_h^1 to

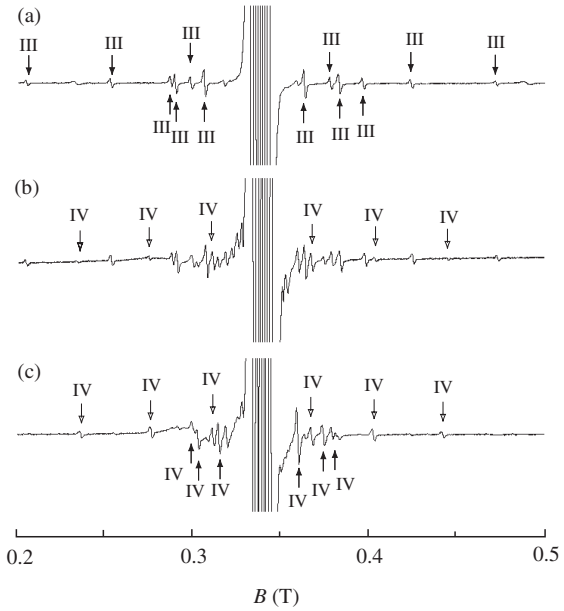

Figure 2. EPR spectra observed at 300 K with $\boldsymbol{B} \parallel [100]$ for the $TlCdF_3$ crystals (a) doped with only Gd, (b) co-doped with Gd and Li, and (c) co-doped with more Li than the crystal in (b).

D_{4h}^{18} structural phase transition at 191 K due to the condensation of a soft phonon mode at the R point of the cubic Brillouin zone [17]. Therefore, we have undertaken EPR experiments on M^{3+} centres in $TlCdF_3$ at room temperature.

In the present paper, we report EPR results for tetragonal Gd^{3+} centres observed in $TlCdF_3$ single crystals doped only with Gd and co-doped with Gd and Li. We focus our attention on the fine-structure splitting in the tetragonal centres. The fine-structure parameters are discussed by comparing the axial parameters b_{2a}, b_{4a} and the cubic parameter b_{4c} for the tetragonal Gd^{3+} centres in $TlCdF_3$ with the corresponding axial and cubic parameters for the same kinds of Gd^{3+} centres in other perovskite fluorides having different monovalent cations.

2. Experimental procedures and results

Single crystals of $TlCdF_3$ doped with gadolinium were grown using the Bridgman technique. As a doped impurity, Gd metal was added to starting mixtures of TlF and CdF_2 powders. In some mixtures a trace of LiF powder was added together with Gd metal. The mixture was sealed in a graphite crucible and melted in argon atmosphere. The crystals obtained were cleaved easily along {100} planes. EPR measurements were carried out at room temperature using an X-band spectrometer (JES-FE1XG, JEOL) with 100 kHz field modulation at the Advanced Instrument and Analysis Division in Nagoya Institute of Technology. Resonant fields were measured accurately with a proton NMR probe EFM-2000 (Echo Electronics).

The EPR measurements were performed at room temperature. Typical recorder traces of EPR spectra are shown in figure 2 with the external magnetic field $\boldsymbol{B}$ parallel to the crystalline [100] axis. Figure 2(a) shows EPR spectra for a $TlCdF_3$ crystal doped only with Gd metal. In the narrow field range near 0.34 T, a spectrum composed of intense signals was observed. The spectrum was found to have cubic symmetry, and is ascribed to the Gd^{3+} centre reported

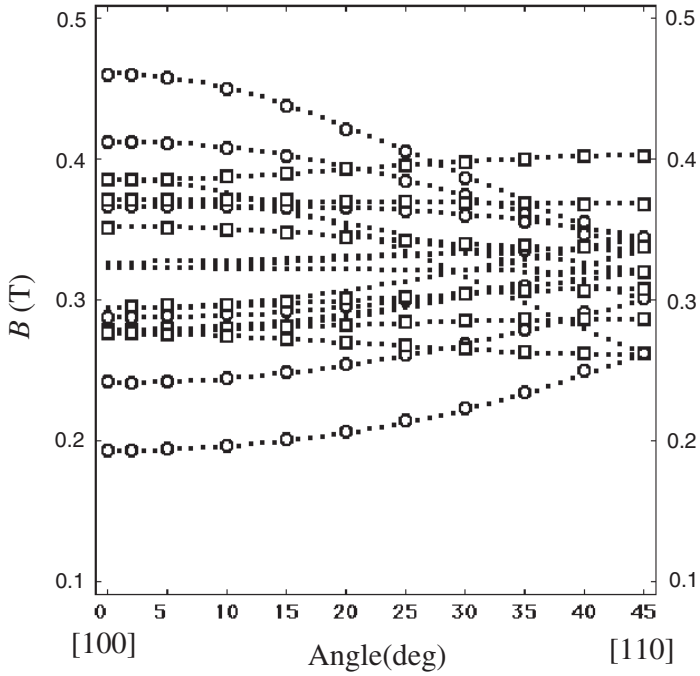

Figure 3. Angular variation of signals marked with III in figure 2(a) with $\boldsymbol{B}$ in the (001) plane. Open circles and squares represent the resonance fields of the signals observed. Dotted curves denote the resonant fields calculated using the parameters for the centre III listed in table 1.

previously by Rewaj *et al* [10], where Gd^{3+} ion is substituting for Cd^{2+} ion without any charge compensator in its immediate neighbourhood (cubic Gd^{3+} centre). Other signals marked with III were observed in a wide range of magnetic field.

Figures 2(b) and (c) show the recorder traces of EPR signals observed for the $TlCdF_3$ crystal co-doped with Gd and Li with $\boldsymbol{B}$ parallel to a [100] direction. The crystal in figure 2(c) is doped with more Li than the crystal in figure 2(b). Signals marked with III seen in figure 2(a) are weakened in figure 2(b) and have disappeared in figure 2(c). Instead, new signals marked with IV were observed by co-doping with Li. In the [100]-field direction, the total splitting of the fine structure for the Gd, Li co-doped crystal is a little smaller than that for the Gd-only-doped crystal.

Angular variations of the signals marked with III in figure 2(a) are shown in figure 3, in which the magnetic field direction is rotated from the [100]-axis to the [110]-axis direction in the (001) plane. This makes it clear that the sets of seven signals observed in figure 3 correspond to fine-structure splittings of a Gd^{3+} centre with spin $S = \frac{7}{2}$, although the central-field signal in the fine structure is overlapping with those from the cubic Gd^{3+} centre. Open squares in figure 3 denote the angular variations of the signals with 90° periodicity, which have peaks and troughs in the [100] and [110] directions. Open circles denote the signals having peaks and troughs in the [100] direction, which have 180° periodicity in the (001) plane. The signals represented by open circles coincide with those represented by open squares in the [010] field direction. The above feature indicate that the Gd^{3+} centre for the signals marked with III have tetragonal symmetry about the crystalline ⟨100⟩ axis (centre III). The tetragonal symmetry results from the association of some local charge compensator along one of the crystalline axes.

Table 1. Spin-Hamiltonian parameters for centres III and IV in $TlCdF_3$ observed at 300 K. The fine-structure parameters b_n^m are in units of 10^{-4} cm^{-1}. Absolute signs of the fine-structure parameters are determined by using the empirical rule $b_{4c} < 0$ as mentioned in the text.

Centre	g	b_2^0	b_4^0	b_4^4	b_6^0	b_6^4
III	1.992(1)	−201.5(2)	−1.96(6)	−33.9(6)	0.70(4)	−23(2)
IV	1.992(1)	−153.6(2)	−2.88(6)	−24.0(7)	0.76(7)	−12(2)

Angular variations of the signals marked with IV in figures 2(b) and (c) in the Gd, Li co-doped crystal show a similar feature to those of the centre III in the Gd-only-doped crystal. This indicates that the Gd^{3+} centre for the signals marked with IV also has tetragonal symmetry about the crystalline ⟨100⟩ axis (centre IV).

The spectra of the centres III and IV can be described by the following spin Hamiltonian with $S = \frac{7}{2}$;

$$\mathcal{H} = g\beta \boldsymbol{S}\cdot\boldsymbol{B} + \tfrac{1}{3}b_2^0 O_2^0 + \tfrac{1}{60}\left[b_4^0 O_4^0 + b_4^4 O_4^4\right] + \tfrac{1}{1260}\left[b_6^0 O_6^0 + b_6^4 O_6^4\right], \qquad (1)$$

where O_2^0, O_4^0, O_4^4, O_6^0 and O_6^4 are the Stevens operators given in [18]. The principal axes are chosen to be parallel to the crystalline ⟨100⟩ axes. The spin Hamiltonian was fitted to the observed spectra using the direct matrix-diagonalization method. The Zeeman term was fitted with an isotropic g tensor within experimental error.

From the fitting of the spin Hamiltonian, only relative signs among the fine-structure parameters b_n^m can be determined. The spin-Hamiltonian parameters obtained for the centres III and IV are tabulated in table 1. The dotted curves in figure 3 show the theoretical curves calculated using the parameters listed in table 1. Good agreement of the calculated values of resonant fields with experimental ones is obtained.

The Gd^{3+} ions are considered to be substituting for Cd^{2+} ions, as a Gd^{3+} ion has ionic radius close to that of a Cd^{2+} ion. For both tetragonal centres III and IV, excess monovalent positive charge on the Gd^{3+} ion may be compensated by some charge compensator at the nearest Cd^{2+} site. This is feasible from the magnitudes of the b_2^0 parameters and from the fact that the signals III disappeared in the Gd, Li co-doped crystal and instead signals IV appeared. Thus, the centre III observed in the Gd-only-doped crystal is ascribed to a Gd^{3+} ion associated with a Cd^{2+} vacancy at the nearest Cd^{2+} site (Gd^{3+}–V_{Cd} centre). On the other hand, the centre IV observed in the Gd, Li co-doped crystal is formed by a Gd^{3+} ion associated with a Li^+ ion at the same nearest Cd^{2+} site (Gd^{3+}–Li^+ centre). Schematic models of these centres are shown in figure 4.

Absolute signs of the parameters b_n^m in table 1 can be determined by considering the cubic components of the fine-structure terms in the spin Hamiltonian (1). We separate the fine-structure terms into uniaxial and cubic terms up to the sixth rank as follows [13]:

$$\begin{aligned}\tfrac{1}{3}b_2^0 O_2^0 + \tfrac{1}{60}\left[b_4^0 O_4^0 + b_4^4 O_4^4\right] + \tfrac{1}{1260}\left[b_6^0 O_6^0 + b_6^4 O_6^4\right] \\ = \tfrac{1}{3}b_{2a} O_2^0 + \tfrac{1}{60}\left[b_{4a} O_4^0 + b_{4c}(O_4^0 + 5O_4^4)\right] \\ + \tfrac{1}{1260}\left[b_{6a} O_6^0 + b_{6c}(O_6^0 - 21O_6^4)\right]. \qquad (2)\end{aligned}$$

The terms in b_{4c} and b_{6c} in equation (2) denote the cubic character of the tetragonal Gd^{3+} centres and are to be compared with those for the cubic Gd^{3+} centre in the same host crystal. The separated parameters obtained are tabulated in table 2 together with the parameters for the cubic Gd^{3+} centre in $TlCdF_3$ reported previously [10]. Since the cubic parameter b_{4c} (=b_4) is negative for the cubic Gd^{3+} centre, we choose the same negative sign of the separated cubic parameters b_{4c} for tetragonal Gd^{3+}–V_{Cd} and Gd^{3+}–Li^+ centres. Thus, the absolute signs of the fine-structure parameters b_n^m are determined as listed in table 1.

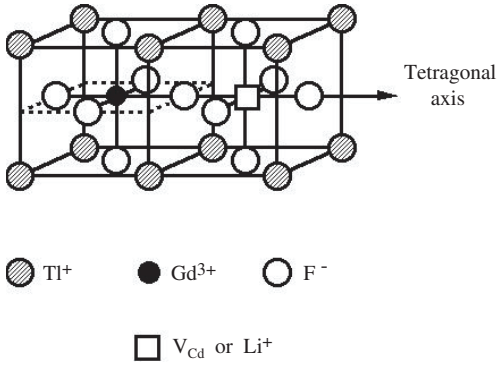

Figure 4. Models of Gd^{3+}–V_{Cd} centre and Gd^{3+}–Li^{+} centre formed in $TlCdF_3$. The open square denotes a Cd^{2+}-ion vacancy for the former and a Li^{+} ion for the latter.

Table 2. Separated fine-structure parameters b_{na} ($n = 2, 4, 6$) and b_{nc} ($n = 4, 6$) and the ratio b_{6c}/b_{4c} obtained at 300 K for Gd^{3+}–V_{Cd} and Gd^{3+}–Li^{+} centres in $TlCdF_3$. Fine-structure parameters b_{4c} ($=b_4$) and b_{6c} ($=b_6$) for the cubic Gd^{3+} centre are listed for comparison. b_{na} and b_{nc} are in units of 10^{-4} cm^{-1}.

Centre	b_{2a}	b_{4a}	b_{4c}	b_{6a}	b_{6c}	b_{6c}/b_{4c}
Gd^{3+}–V_{Cd}	−201.5	4.82	−6.78	−0.40	1.1	−0.16
Gd^{3+}–Li^{+}	−153.6	1.92	−4.80	0.19	0.57	−0.12
Gd^{3+} [a]	—	—	−3.49		0.72	−0.21

[a] Reference [10] (observed at 297 K).

The b_{4c} and b_{6c} values for the Gd^{3+}–Li^{+} centre are closer to the values for the cubic centre as compared with those for the Gd^{3+}–V_{Cd} centre. The magnitudes of the axial parameters b_{2a} and b_{4a} for the Gd^{3+}–Li^{+} centre are considerably smaller than those for the Gd^{3+}–V_{Cd} centre.

3. Discussion

3.1. Axial fine-structure parameters

In a previous paper [7], Arakawa *et al* reported the separated axial and cubic fine-structure parameters for the same kinds of tetragonal Gd^{3+}–V_{Cd} and Gd^{3+}–Li^{+} centres in perovskite fluorides $KCdF_3$, $RbCdF_3$, $CsCdF_3$, $RbCaF_3$ and $CsCaF_3$. In table 3, the separated axial parameters b_{na} ($n = 2, 4$) in $TlCdF_3$ are compared with those in these perovskite fluorides.

As seen from table 3, the magnitudes of the axial parameters b_{2a} for Gd^{3+}–V_{Cd} and Gd^{3+}–Li^{+} centres are much smaller in $TlCdF_3$ than those in other perovskite fluorides. In particular, the magnitude of b_{2a} for the Gd^{3+}–Li^{+} centre in $TlCdF_3$ is about one-half of that for $RbCdF_3$ in spite of their close lattice constants. The anomalously small magnitude of b_{2a} for the Gd^{3+}–Li^{+} centre in $TlCdF_3$ possibly arises from the decrease in the difference of the local deviations between the ligands parallel and normal to the tetragonal axis. The neighbouring Tl^{+} ions might contribute to this decrease.

Additional information about the tetragonal Gd^{3+} ($S = \frac{7}{2}$) centres can be obtained from the fourth-rank axial parameter b_{4a}, which is absent in the Cr^{3+} ($S = \frac{3}{2}$) centre. As seen from table 3, the b_{4a} value for the Gd^{3+}–Li^{+} centre in $TlCdF_3$ is about one-half of that for $RbCdF_3$. This behaviour is similar to the case of b_{2a}.

Table 3. Comparison of the separated axial b_{na} ($n = 2, 4$) and cubic b_{4c} parameters for Gd^{3+}–V_B (B = Cd, Ca) and Gd^{3+}–Li^+ centres in several cubic perovskite fluorides, together with b_4 for cubic Gd^{3+} centres in the same host crystals. The fine-structure parameters are in units of 10^{-4} cm^{-1}.

Host crystal	Lattice const. a (Å)	Cubic centre b_4	V_B centre			Li^+ centre		
			b_{2a}	b_{4a}	b_{4c}	b_{2a}	b_{4a}	b_{4c}
$KCdF_3$[a]	4.327	−1.6[c]	−248.9	4.88	−5.18	−268.0	4.09	−4.60
$RbCdF_3$[a]	4.395	−4.44[d]	−291.3	6.20	−8.32	−330.2	5.26	−7.66
$TlCdF_3$[b]	4.400	−3.49[e]	−201.5	4.82	−6.78	−153.6	1.92	−4.80
$RbCaF_3$[a]	4.456	−4.92[f]	−274.9	5.72	−8.58	−318.2	5.84	−8.80
$CsCdF_3$[a]	4.460	−4.82[d]	−315.1	6.90	−9.28	−379.8	7.14	−9.40
$CsCaF_3$[a]	4.524	−5.49[d]	−314.7	6.91	−9.96	−388.3	8.17	−10.88

[a] Reference [7]; [b] This work; [c] Rerefence [2]; [d] Reference [5]; [e] Reference [10]; [f] Reference [4].

3.2. *Cubic fine-structure parameter*

For the tetragonal Gd^{3+} centres, information about the local deviations of the ligand F^- ions in the plane normal to the tetragonal axis can be obtained from the separated cubic parameter b_{4c}. Table 3 shows the b_{4c} values for each tetragonal Gd^{3+} centre in comparison with corresponding parameter b_4 for the cubic Gd^{3+} centre in the same host crystal. Anomalies in the magnitude of b_{4c} are revealed for both Gd^{3+}–V_{Cd} and Gd^{3+}–Li^+ centres in $TlCdF_3$. In particular, the magnitude of b_{4c} for the Gd^{3+}–Li^+ centre in $TlCdF_3$ is rather small compared with that for the Gd^{3+}–Li^+ centre in $RbCdF_3$, similarly to the case of the axial parameters b_{2a} and b_{4a}.

In $ACdF_3$ (A = K, Rb, Cs) series, the $|b_{4c}|$ and $|b_4|$ values increase with lattice constant. The small magnitude of b_4 in $TlCdF_3$ suggests that the GdF_6 complex may be a compact one with shorter Gd^{3+}–F^- bond length than that in $RbCdF_3$. The small magnitudes of b_{4c} for Gd^{3+}–V_{Cd} and Gd^{3+}–Li^+ centres in $TlCdF_3$ also suggest that the bond lengths of the ligands normal to the tetragonal axis may be shorter than those in $RbCdF_3$.

3.3. *Differences of the axial and cubic parameters between two tetragonal centres*

Here, we examine the behaviour of the differences between the separated parameters b_{na} or b_{4c} for Gd^{3+}–V_B centres (B = Cd, Ca) and corresponding values for Gd^{3+}–Li^+ centres defined by

$$\Delta|b_{2a}| \equiv |b_{2a}(V_B)| - |b_{2a}(Li^+)|, \tag{3}$$

$$\Delta|b_{4a}| \equiv |b_{4a}(V_B)| - |b_{4a}(Li^+)|, \tag{4}$$

$$\Delta|b_{4c}| \equiv |b_{4c}(V_B)| - |b_{4c}(Li^+)|. \tag{5}$$

The differences and the ratios $\Delta|b_{4a}|/\Delta|b_{4c}|$ in several perovskite fluorides are given in table 4. Variation of $\Delta|b_{2a}|$ against lattice constant is shown in figure 5, where $\Delta|b_{2a}|$ values for Cr^{3+} centres [12] are plotted for comparison. Both $\Delta|b_{2a}|$ (Gd) and $\Delta|b_{2a}|$ (Cr) values have negative sign and decrease monotonically with lattice constant in the series of $KCdF_3$–$RbCdF_3$–$CsCdF_3$. The negative sign indicates that the magnitude of b_{2a} for the M^{3+}–Li^+ centre is larger than that for M^{3+}–V_{Cd} centre, although the effective negative charge on the Li^+ ion is one-half of that on the vacancy at the same nearest Cd^{2+} site.

Contrary to the prediction from the variation curve for $ACdF_3$ with monovalent cations (A = K^+, Rb^+ and Cs^+), the $\Delta|b_{2a}|$ value in $TlCdF_3$ has opposite sign, as shown in figure 5. That is, the magnitude of b_{2a} for the Gd^{3+}–V_{Cd} centre is larger than that for the Gd^{3+}–Li^+ centre in $TlCdF_3$. This tendency in thallium compounds is similar to the case of

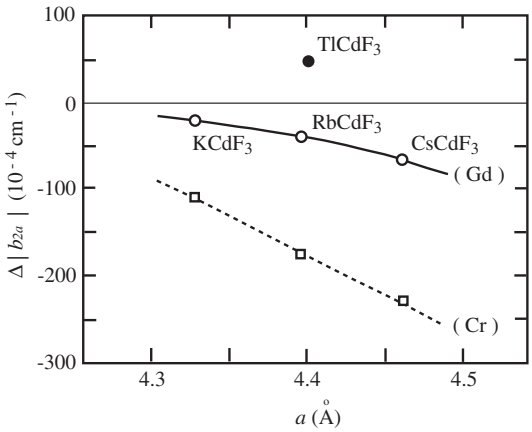

Figure 5. Variations of $\Delta|b_{2a}|$ for Gd^{3+} centres (open circles) and for Cr^{3+} centres [12] (open squares) against lattice constant a in $ACdF_3$ (A = K, Rb, Cs). The value of $\Delta|b_{2a}|$ for Gd^{3+} centres in $TlCdF_3$ is plotted by a closed circle. Solid and dotted lines are guides for the eyes.

Table 4. Values of the differences defined in equations (3)–(5) and the ratio of $\Delta|b_{4a}|/\Delta|b_{4c}|$ in several cubic perovskite fluorides. The differences are in units of 10^{-4} cm^{-1}.

Crystal	$\Delta\|b_{2a}\|$	$\Delta\|b_{4a}\|$	$\Delta\|b_{4c}\|$	$\Delta\|b_{4a}\|/\Delta\|b_{4c}\|$
$KCdF_3$	−19.1	0.79	0.58	1.4
$RbCdF_3$	−38.9	0.94	0.66	1.4
$TlCdF_3$	47.9	2.9	1.98	1.5
$RbCaF_3$	−43.3	−0.12	−0.22	0.54
$CsCdF_3$	−64.7	−0.24	−0.12	2.0
$CsCaF_3$	−73.6	−1.26	−0.92	1.4

$\Delta|b_{2a(2)}|$ for the Cr^{3+} centres reported previously in layered perovskite fluorides [14], where $\Delta|b_{2a(2)}| = +468.2\times10^{-4}$ cm^{-1} in Tl_2ZnF_4 and $\Delta|b_{2a(2)}| = -47.1\times10^{-4}$ cm^{-1} in Rb_2ZnF_4. As seen in table 4, the $\Delta|b_{4a}|$ value in $TlCdF_3$ has the same positive sign as that in $RbCdF_3$, in contrast with $\Delta|b_{2a}|$. These different behaviours of $\Delta|b_{2a}|$ and $\Delta|b_{4a}|$ indicate that the contribution of local distortion to b_{2a} differs from that to b_{4a}.

On the other hand, the variation of $\Delta|b_{4a}|$ value in various perovskite fluorides is very similar to that of $\Delta|b_{4c}|$. The ratio $\Delta|b_{4a}|/\Delta|b_{4c}|$ (=1.5) for $TlCdF_3$ in table 4 is close to those (=1.4) in different host crystals except for $RbCaF_3$ and $CsCdF_3$, where the values of the differences themselves are very small. It must be emphasized that the agreement of the ratio $\Delta|b_{4a}|/\Delta|b_{4c}|$ occurs over the host crystals having various signs and magnitudes of $\Delta|b_{4c}|$ and $\Delta|b_{4a}|$ values. This suggests that the lattice-constant dependences of b_{4a} and b_{4c} arise from the same origin.

The ligand ions in the plane normal to the tetragonal axis contribute to the b_{4c} values. The $\Delta|b_{4a}|$ and $\Delta|b_{4c}|$ values for $TlCdF_3$ are respectively about three times larger than those for $RbCdF_3$, as shown in table 4. The bond length to the ligand in the normal plane for the Gd^{3+}–V_{Cd} centre may become longer than that for the Gd^{3+}–Li^+ centre in $TlCdF_3$ by coulomb repulsion with the intervening F^- ion deviated more closely to the Gd^{3+} ion due to a divalent deficient charge on the Cd^{2+} vacancy. The neighbouring Tl^+ ions make it easier to deviate the ligands in the normal plane than Rb^+ ions.

For a rare-earth ion in a coordination with a lack of inversion symmetry, the odd terms of the crystal field mix the states of opposite parity, such as $4f^{n-1}5d$, into the $4f^n$ manifold. It has been shown by Kiel [19] that the odd crystal field gives rise to second-order contributions to the fine-structure splitting. Bijvank *et al* [20] applied the second-order effects of the odd crystal field to the analysis of the values of b_2^0 parameters determined by EPR experiments for the Gd^{3+} complexes in CaF_2-like crystals. There, the contribution to b_2^0 from the odd crystal field was estimated as a considerable opposite effect against that from the even crystal fields. Arakawa *et al* [21] reported EPR results for two kinds of tetragonal Gd^{3+} centre formed at different cation sites in the layered perovskite crystal Tl_2ZnF_4, where one is at the Tl^+ site with a lack of inversion symmetry and the other is at the Zn^{2+} site with inversion symmetry. The magnitude of the ratio b_{4a}/b_{2a} for the centre without inversion symmetry was about three times larger than that with inversion symmetry.

In the present tetragonal Gd^{3+} centres with a lack of inversion symmetry in cubic perovskite crystals, the odd crystal field along the tetragonal axis arises from the charge compensator. The parameter b_{2a} is sensitive to the odd-crystal-field effect through the effective charge of the charge compensator and the local distortion of the intervening F^- ion along the tetragonal axis. On the other hand, $\Delta|b_{4a}|$ shows very similar dependence on the lattice constant to $\Delta|b_{4c}|$ which is caused by ligands in the plane normal to the tetragonal axis. This fact shows that the parameter b_{4a} is insensitive to the odd crystal field. The results are consistent with the fact reported in Tl_2ZnF_4 [21] that the magnitude of the ratio b_{4a}/b_{2a} for the tetragonal Gd^{3+} centre without inversion symmetry is larger than that for the centre with inversion symmetry. The large magnitude of the ratio b_{4a}/b_{2a} for a centre with a lack of inversion symmetry is considered to be related to the reduction of $|b_{2a}|$ by the odd-crystal field effect.

4. Conclusion

Two tetragonal centres were detected by room-temperature EPR measurements on Gd-doped $TlCdF_3$ crystals. One centre observed in the Gd-only-doped crystal of $TlCdF_3$ is identified to be a Gd^{3+}–V_{Cd} centre, where a Gd^{3+} ion is substituted for a Cd^{2+} ion and is associated with a nearest-Cd^{2+} vacancy on the tetragonal axis. The other centre observed in the Gd, Li co-doped crystal is identified to be a Gd^{3+}–Li^+ centre, where a Gd^{3+} ion is substituted for a Cd^{2+} ion and is associated with a Li^+ ion at the same nearest-Cd^{2+} ion site. For these centres, the spin-Hamiltonian parameters have been determined accurately by the direct matrix-diagonalization method. The obtained fine-structure parameters are separated into the axial parameters (b_{2a}, b_{4a}, b_{6a}) and the cubic parameters (b_{4c}, b_{6c}).

The axial parameters b_{2a}, b_{4a} and the cubic parameter b_{4c} for the Gd^{3+}–V_{Cd} centre and the Gd^{3+}–Li^+ centre in $TlCdF_3$ have anomalous values distinct from those for the corresponding centres in $RbCdF_3$ in spite of their close lattice constants. In particular, the magnitudes of these parameters for the Gd^{3+}–Li^+ centre in $TlCdF_3$ have about one-half the magnitudes of those in $RbCdF_3$.

The value of $\Delta|b_{2a}|$ ($=|b_{2a}(V_{Cd})| - |b_{2a}(Li)|$) in $TlCdF_3$ has different sign from that in $RbCdF_3$, in contrast with those of $\Delta|b_{4a}|$ and $\Delta|b_{4c}|$ having the same signs. The agreement of the ratio $\Delta|b_{4a}|/\Delta|b_{4c}|$ in various perovskite fluorides suggests that the lattice-constant dependence of b_{4a} arises from the same origin as that of b_{4c}. The above anomalies for the Gd^{3+}–Li^+ centre in $TlCdF_3$ are considered to result from the deviations of ligand F^- ions in the Tl^+ compounds. The behaviour of b_{2a} may be due to the anomalous local deviation of the intervening F^- ion between the Gd^{3+} and Li^+ ions in the Gd^{3+}–Li^+ centre. On the other hand, the behaviour of b_{4a} or b_{4c} may be due to the anomalous local deviation of the four ligands in the plane normal to the tetragonal axis.

References

[1] Rousseau J J, Gesland J Y, Binois M and Fayet J C 1974 *C. R. Acad. Sci.* B **279** 103–5
[2] Arakawa M, Ebisu H, Yosida T and Horai K 1979 *J. Phys. Soc. Japan* **46** 1483–7
[3] Buzaré J Y, Fayet-Bonnel M and Fayet J C 1980 *J. Phys. C: Solid State Phys.* **13** 857–63
[4] Buzaré J Y, Fayet-Bonnel M and Fayet J C 1981 *J. Phys. C: Solid State Phys.* **14** 67–81
[5] Arakawa M, Aoki H, Takeuchi H, Yosida T and Horai K 1982 *J. Phys. Soc. Japan* **51** 2459–63
[6] Takeuchi H and Arakawa M 1984 *J. Phys. Soc. Japan* **53** 376–80
[7] Arakawa M, Ebisu H and Takeuchi H 1985 *J. Phys. Soc. Japan* **54** 3577–83
[8] Takeuchi H, Arakawa M and Ebisu H 1987 *J. Phys. Soc. Japan* **56** 3677–82
[9] Takeuchi H, Ebisu H and Arakawa M 1995 *J. Phys.: Condens. Matter* **7** 1417–26
[10] Rewaj T, Krupski M, Kuriata J and Buzaré J Y 1992 *J. Phys.: Condens. Matter* **4** 9909–18
[11] Takeuchi H and Arakawa M 1983 *J. Phys. Soc. Japan* **52** 279–83
[12] Arakawa M, Ebisu H and Takeuchi H 1986 *J. Phys. Soc. Japan* **55** 2853–8
[13] Takeuchi H, Arakawa M and Ebisu H 1987 *J. Phys. Soc. Japan* **56** 4571–80
Takeuchi H, Arakawa M and Ebisu H 1990 *J. Phys. Soc. Japan* **59** 2297 (erratum)
[14] Arakawa M, Ebisu H and Takeuchi H 2002 *J. Phys.: Condens. Matter* **14** 8613–23
[15] Arakawa M, Okamoto A, Ebisu H and Takeuchi H 2006 *J. Phys.: Condens. Matter* **18** 3053–67
[16] Takeuchi H, Arakawa M and Ebisu H 1991 *J. Phys.: Condens. Matter* **3** 4405–20
[17] Rousseau M, Gesland J Y, Julliard J, Nouet J, Zarembowitch J and Zarembowitch A 1975 *Phys. Rev.* B **12** 1579–90
[18] Abragam A and Bleaney B 1970 *Electron Paramagnetic Resonance of Transition Ions* (Oxford: Clarendon)
[19] Kiel A 1966 *Phys. Rev.* **148** 247–56
[20] Bijvank E J, Den Hartog H W and Andriessen J 1977 *Phys. Rev.* B **16** 1008–19
[21] Arakawa M, Nakano T, Ebisu H and Takeuchi H 2003 *J. Phys.: Condens. Matter* **15** 3779–92